CONF-951026--12

UCRL-JC- 121912
PREPRINT

HIGH TEMPERATURE DEFORMATION IN 2036 Al AND 0.2 WT.% Zr-2036 Al

J. S. Huang
A. J. Schwartz
T. G. Nieh

This paper was prepared for submittal to
1995 Fall TMS Symposium on Aluminum and
Magnesium for Automotive Applications
in Cleveland, OH on October31-November 2, 1995.

November 1995

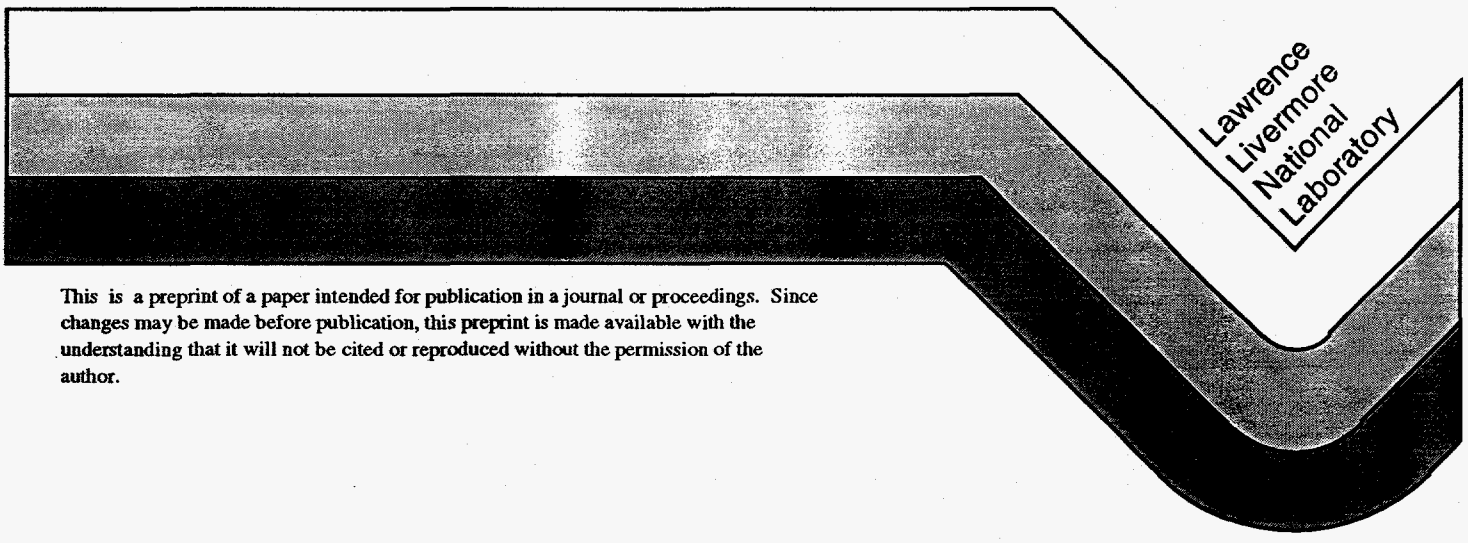

High Temperature Deformation in 2036 Al and 0.2 wt% Zr–2036 Al

J. S. Huang, A.J. Schwartz, and T.G. Nieh

Lawrence Livermore National Laboratory
L–352, P.O. Box 808, Livermore, CA 94551–9900

Abstract

The microstructure and high temperature deformation behavior of 2036 Al and a 0.2 wt% Zr modified 2036 Al were characterized. A particle–simulated–nucleation (PSN) process was applied to refine the grain structure in both alloys. Thermomechanically-processed materials were tested at temperatures from 450 to 500°C and strain rates from 2×10^{-1} to 2×10^{-4} s^{-1}. Strain rate sensitivity exponent, activation energy, and total elongation were measured, and the deformation mechanism was proposed. The effect of Zr on the microstructure and deformation behavior of 2036 Al at elevated temperatures was discussed.

Introduction

The most effective way of increasing automobile mileage while decreasing emissions is to reduce vehicle weight. For example, given existing engine technology, a 30% vehicle weight reduction would be required to boost average mileage to 40 mpg. Aluminum has only about one–third the density of steel, and most commercial Al alloys do possess substantially higher specific strength compared to steel. Also, aluminum is readily recyclable. A vehicle weight reduction would not only result in huge oil/gasoline savings, but also cause a significant reduction in emission.

There is currently a strong desire to use significantly more aluminum to replace steels in automotive body applications for the reasons of lower weight and higher fuel efficiency. However, there exist several obstacles to the introduction of aluminum sheet components. Obstacles include the relatively high cost of aluminum as compared to steels and the development of cost effective methods for bonding. Other problems arise when one tries to form aluminum panels with the existing technology that has been optimized for sheet steel. These include: 1) The forming limits of aluminum are significantly lower than those for steel. Aluminum is particularly prone to tearing at bends. This limits the shapes that can be fabricated and slows die design, die tryout and application. 2) Thicker aluminum sheets are required to produce the same strength as a steel component; as such springback is more severe and it is difficult to keep dimensional tolerances. 3) Traditional vehicle body manufacturing technology utilizing stamped sheet steel components cannot be sufficiently improved to meet future vehicle requirements because of the inherent weight of steel and the high cost and long time necessary for stamping tool development. It would be desirable if at least prototypes could be produced with one–sided die sets. This would accelerate the time–to–market.

As a result of this there is renewed interest in superplasticity, and particularly high rate superplastic forming to form auto body components. These techniques have the advantages of delivering exceptional formability, potentially giving good dimensional tolerance and delivering rapid time–to–market as one–sided dies are employed. There are some potentially drawbacks with this technique as well. For example, for low–strength aluminum (e.g., 5083 Al), the as–formed components may not have acceptable mechanical properties. For high–strength aluminum (e.g., 2000 series Al), additional heat treatments may be necessary for as–formed components, which may affect their dimensional accuracy. In addition, cavitation as a result of superplastic forming and its influence upon the subsequent mechanical properties may be of great concern. These issues are some of the major barriers for the economical development of this technology for mass production.

Several 2000 series Al, e.g., 2024, 2124, 2618, and SUPRAL alloys, have been demonstrated to be superplastic [1–5]. These alloys are noted to contain high Cu (~4–5 wt%), while typical alloys used for the automotive bodies have a much lower Cu content, e.g., 2036 Al. Despite the fact that these latter alloys are less expensive, easier to make, they have not been demonstrated to be superplastic. There exist limited data for Al alloys illustrating the relationship between tensile elongation and Cu content, as shown in Fig. 1 [3, 6]. Although the data indicate that for optimum ductility the Cu content is about 4 wt%, a tensile elongation of over 400% can be readily achieved in alloys which contain only 2 wt% Cu. The typical plastic strain for conventional forming operations, even to form a complex part, is about 100%. A 400% ductility well exceeds this strain requirement.

According to Fig. 1, 2036 Al (nominal composition by weight%: 2.6Cu–0.45Mg–0.25Mn) is expected to have good formability. It is pointed out, however, that all the data in Fig. 1 were obtained from fine–grained (~5 μm) materials. Conventional 2036 Al is not fine–grained; its grain size, depending upon annealing conditions, is approximately 20 to 50 μm. Manganese has traditionally been used as the grain refining element. It is now recognized that Zr is a more effective grain refiner for aluminum (forms Al_3Zr precipitates). For example, it was reported in 1970 [7] that a Russian alloy (V96Ts) that is rather similar in composition to the 7000 series alloys, but contains Zr as a grain refining element instead of Cr, has a finer grain size (~5 μm) than 7456 Al (~12 μm). The Zr–containing alloy exhibits a superplastic strain rate that is about 100 times faster than that of the Cr–containing alloy. The grain size of a properly thermomechanically–processed 2036 Al is expected to be in the range of 2–5 μm, if Zr was used to replace Mn. In such a case, data in Fig. 1 are directly applicable to 2036 Al, and the fine-grained alloy would exhibit an elongation value of over 500%. Furthermore, resulting from having a finer grain size, strain rate to produce large elongation is also expected to increase to a higher value [8].

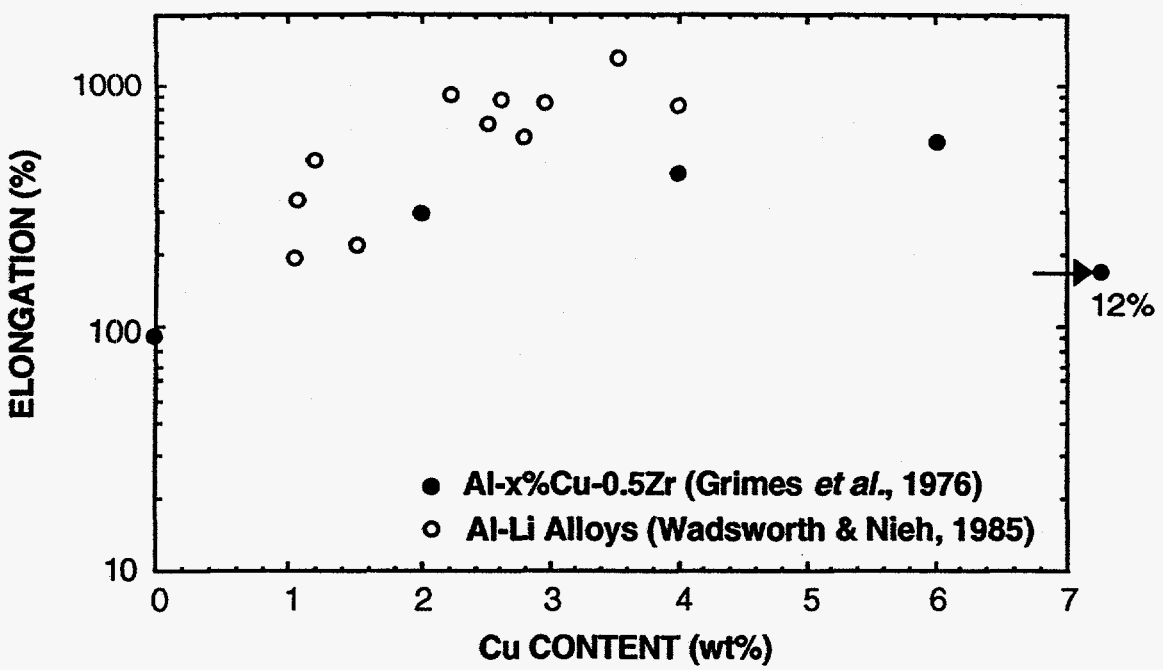

Fig. 1 Elongation of aluminum alloys as a function of Cu content. Even at 1 wt% Cu, the elongation value can still be over 300%.

The purpose of this work is to investigate the effects of Zr addition in the conventional 2036 Al alloy on its microstructure during thermomechanical processing and high temperature deformation. Although Zr addition to aluminum alloys has been studied in many powder–metallurgy aluminum [3, 9–11], limited work has been performed on ingot–metallurgy products.

Materials and Experiments

Two alloys were chosen for this study to investigate the effect of Zr addition on microstructure and tensile properties of 2036 Al alloy. Chemical compositions of the two alloys are listed in Table 1. The first alloy is the conventional 2036 Al and the second alloy is 2036 Al with a 0.21 wt% Zr addition (denoted Zr–2036 Al). Both alloys were cast by Kaiser Aluminum as 75 mm x 600 mm x 900 mm rectangular billets.

Table 1. Chemical Composition (wt%) of Studied Alloys.

Alloy	Cu	Mg	Mn	Zr	Fe	Si	Al
2036 Al	2.72	0.44	0.27	0	0.27	0.29	Balance
Zr–2036 Al	2.63	0.43	0.25	0.21	0.26	0.29	Balance

A particle–simulated–nucleation (PSN) process was used to produce fine–grained structure [12]. The process involved first to hot forge the cast alloys to 15 mm thick and, then, roll to 5 mm thick. The forging and rolling temperatures were 500 and 450°C, respectively. The rolled plates were further annealed (i.e. solutioned) at 480°C for 4h, followed by aging the plates in a furnace with the temperature being gradually increased from room temperature to 380°C in 20h. (The latter aging step is to induce the formation of micron–sized Al_2Cu precipitates.) After aging, the plates were additionally cold–rolled to about 2 mm thick, from which tensile samples were machined with their longitudinal axis being along the rolling direction. The above thermomechanical processing is schematically illustrated in Fig. 2.

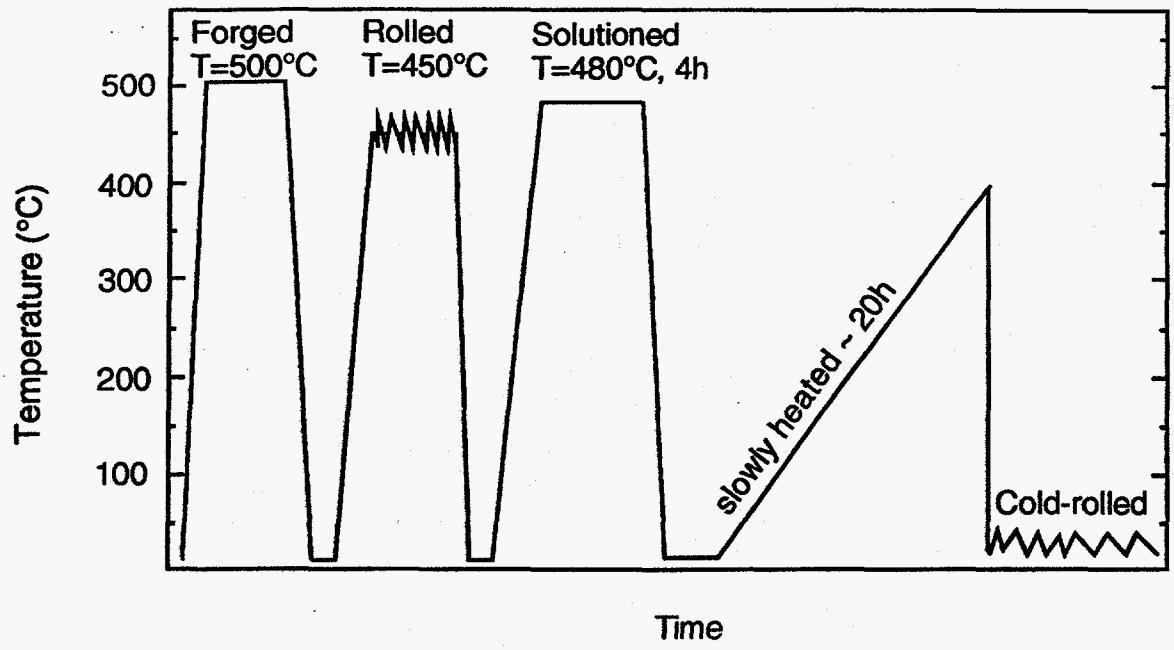

Fig. 2 Schematic illustration of thermomechanical processes for 2036 Al and Zr–2036 Al.

Tensile tests were conducted using an MTS machine attached with a radiant furnace. Typically, a sample was heated from room temperature to the testing temperature in about 1.2 ks. Test temperature ranges from 450°C to 500°C, and strain rate from 2×10^{-4} to 2×10^{-1} s^{-1}. The microstructure of samples both prior to and after testing were examined with conventional optical microscopy. Transmission electron microscopy was also used to examine precipitate size and distribution in the materials.

Results

Microstructure

The grain structures of the two alloys after solutioning are quite similar, as shown in Fig. 3; grains are elongated and coarse. Typical widths of the grains are about 40–60 μm and the lengths are more than 100 μm. Many large inclusions are also observed in the microstructures. These inclusions (Fig. 4) generally appear as stringers distributed both within grains and along grain boundaries. These inclusions are typically 5 μm long by 2 μm wide. Energy dispersive (EDS) analysis indicates that these inclusions are Fe and Cu–rich particles. In addition to these coarse inclusions, Al_2Cu (as well as Al_6Mn) precipitates were found in the microstructure, suggesting that the solution temperature (480°C) was insufficient to completely dissolve Cu into aluminum matrix. The sizes of Al_6Mn and Al_2Cu particles range between 50 and 200 nm.

The aging treatment (i.e., PSN) is expected to produce a uniform distribution of fine Al_2Cu precipitates in both alloys. However, despite the addition of a 0.21 wt% Zr, experimental results showed that there exists an insignificant difference between the aged microstructures, e.g., grain size and morphology, in the two alloys. Typical optical photomicrographs of the aged alloys are given in Fig. 5. The aging treatment results in the formation of 100 to 300 nm Al_6Mn precipitates at grain boundaries as well as Al_2Cu precipitates in grain interiors. The morphology of the grain boundary precipitates is often lens–shaped while the intragranular precipitates vary from slightly elongated cubes to laths. Figures 6(a) and (b) represent a bright–field/dark–field pair of intragranular Al_2Cu precipitates. The small particle is 180 nm long by 100 nm wide and the larger precipitate is 340 nm long by 160 nm wide. The average Al_2Cu spacing is 900 nm.

Very fine Al_3Zr precipitates (20 to 60 nm) are also observed in the Zr–modified alloy (Fig. 7). Interestingly, these precipitates are detected mainly within grain interior, rather than at grain boundaries, suggesting they are ineffective in pinning grain boundaries.

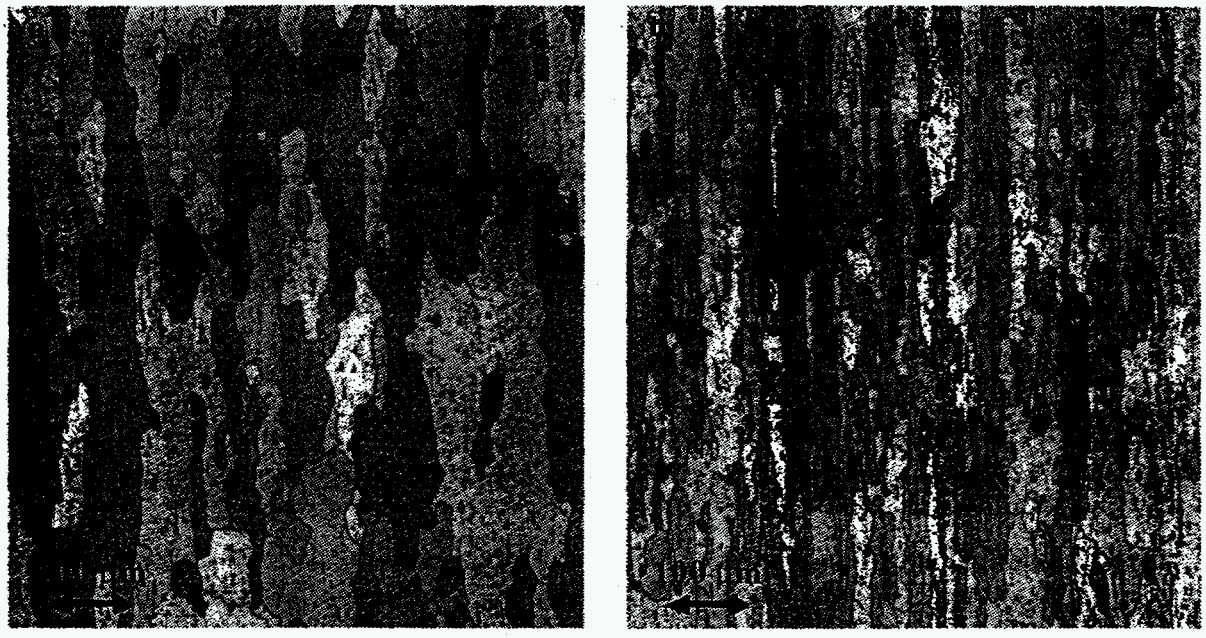

Fig. 3. Optical micrograph of the typical microstructure of (a) 2036 and (b) Zr–2036 Al after the solution treatment.

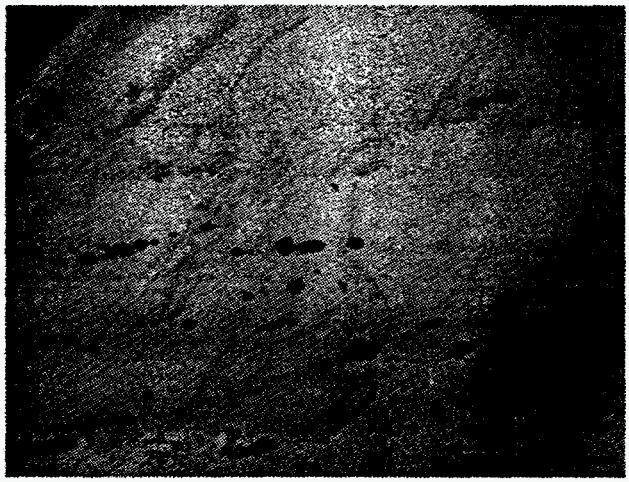

Fig. 4. Fe and Cu–rich inclusions present in 2036 Al solutioned at 480°C.

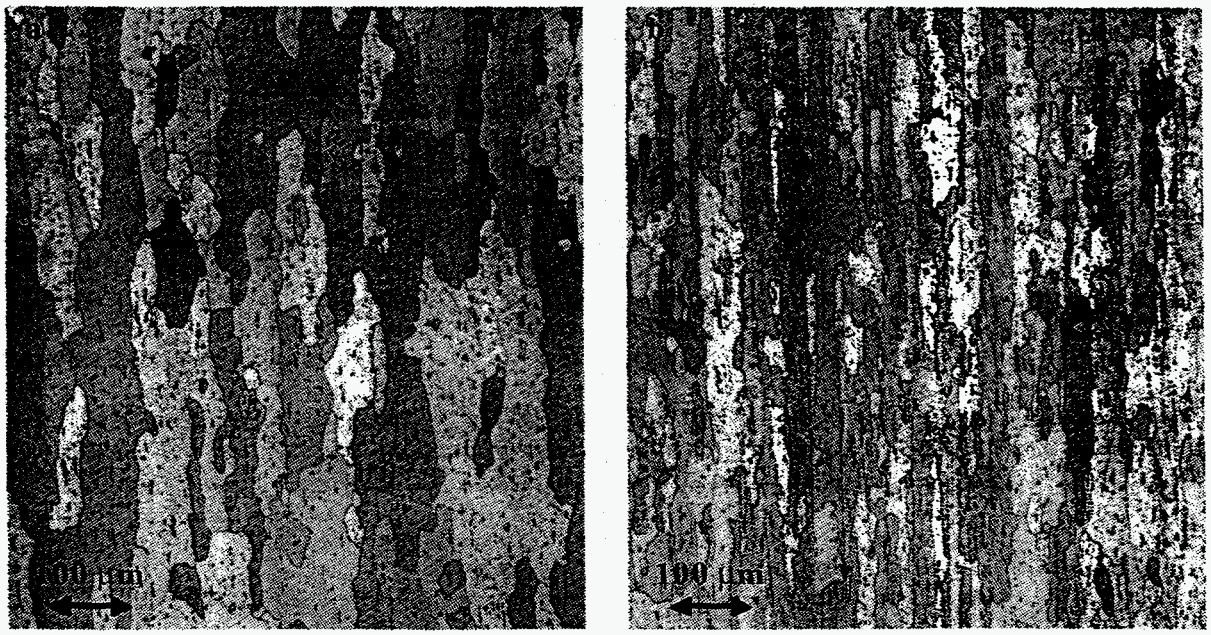

Fig. 5 Microstructure of (a) 2036 and (b) Zr–2036 Al after aging treatment.

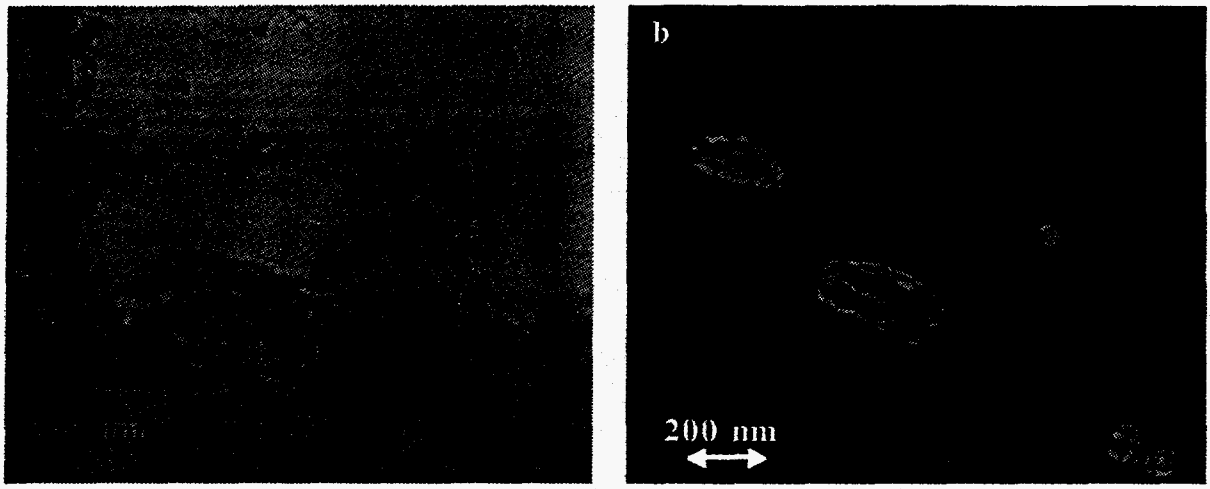

Fig. 6 Al_2Cu precipitates in 2036 Al (a) Bright–field image and (b) dark–field image. The small particle is 180 nm long by 100 nm wide and the larger precipitate is 340 nm long by 160 nm wide.

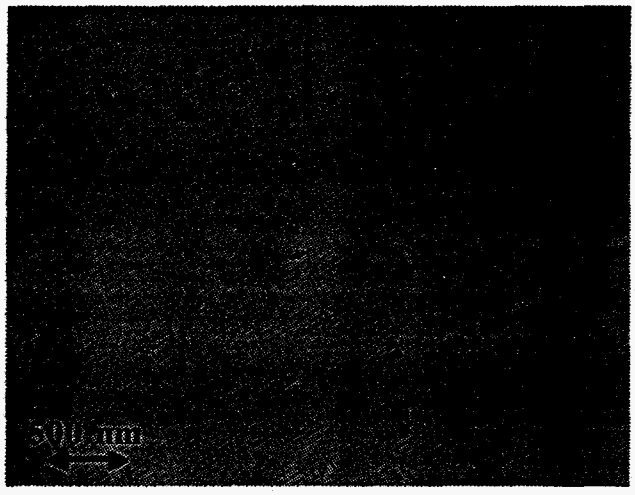

Fig. 7. 20 to 60 nm spherical Al_3Zr precipitates revealed in a bright–field image.

The microstructure of tested samples at areas both near fracture tip and grip area were examined. For both alloys tested at 450°C, the grip areas of the samples (represents static anneal) were not fully recrystallized after testing; the microstructures consist of a mixture of partially–recrystallized and non–recrystallized grains. Even grains in regions where grain structures are clearly developed are elongated. The widths of these grains range from 10 to 40 μm, and the lengths from 20 to 100 μm. There is, again, no substantial difference in grain structure between the two alloys, suggesting Zr has an insignificant effect on microstructural refinement. The grain structure of the two alloys at areas near fracture tip (represents dynamic anneal) are also similar. All the samples except those tested at 2×10^{-4} s^{-1} were only partially recrystallized. For the samples tested at 2×10^{-4} s^{-1}, elongated grains with widths ranging from 5 to 20 μm and lengths ranging from 5 to 100 μm were observed. It is particularly noted that extensive grain boundary cavitation was observed in both alloys, especially at strain rates less than 2×10^{-3} s^{-1}.

For samples tested at 500°C, the recrystallization of grains at both grip area and fracture tip was found to be at a greater extent. However, there is no indication of dynamic recrystallization. Microstructure of both alloys are, again, quite similar.

Mechanical Properties

The true stress–true strain curves for 2036 Al and Zr–2036 Al tested at 500°C and a strain rate of 2 x 10^{-3} s^{-1} are shown in Fig. 8. Both alloys exhibit a small work hardening region and rapidly reach an apparent steady state. The curves in Fig. 8 also indicate that sample necking prior to fracture is insignificant, consistent with the fact that these alloys have a relatively low strain rate sensitivity exponent (shown later).

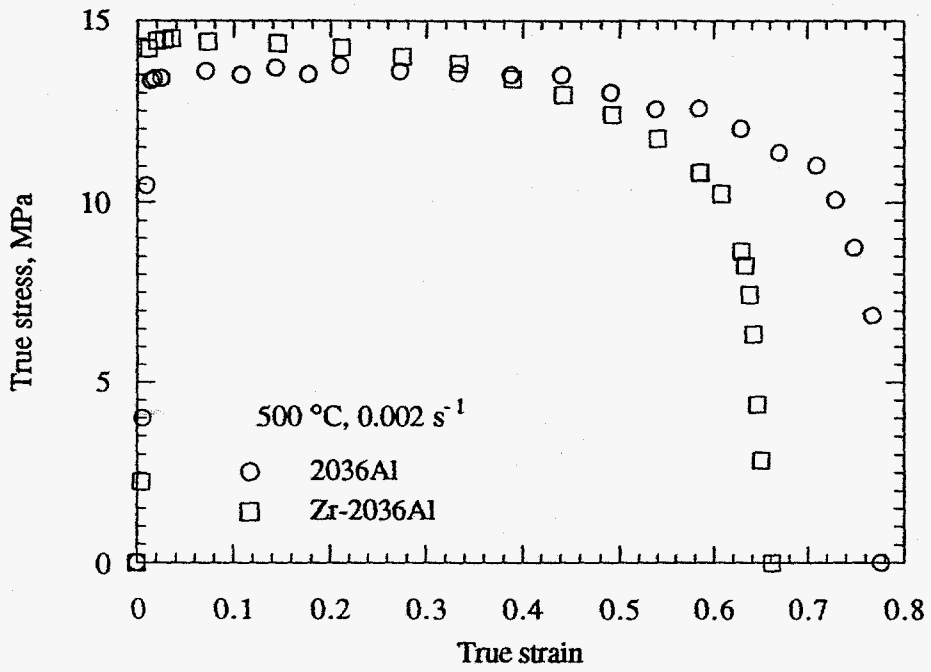

Fig. 8. Comparison of true stress–true strain curves between 2036 Al and Zr–2036 Al at 500°C and a strain rate of 2 x 10^{-3} s^{-1}.

The steady–state flow stress at 475°C plotted as a function of strain rate for the two alloys is shown in Fig. 9. Despite a slight difference in flow stresses, the strain rate sensitivity exponent, m, is noted to be almost the same for the two alloys. Similar observation was also made at 450 and 500°C. Specifically, the m value ranges from 0.13 to 0.19 for 2036 Al, and from 0.14 to 0.17 for Zr–2036 Al. This result indicates that the 0.21 wt% Zr addition does not produce an appreciable effect on the high–temperature deformation behavior in 2036 Al.

To assess the temperature dependence of plastic flow, Fig. 10 shows the normalized strain rate $(\dot{\varepsilon}/(\sigma/E)^5)$ as a function of the reciprocal of temperature for both alloys. The activation energies, Q, were determined to be 163 and 178 kJ/mole for 2036 and Zr–2036 Al, respectively. These activation energies are noted to be close to the activation energy for self–diffusion in Al, 143 kJ/mole [13]. The results that the strain rate sensitivity is relatively low (~0.2) and the activation energy is close to that of self–diffusion in Al suggest a recovery–type mechanism (e.g., dislocation climb) is responsible for high–temperature deformation in these alloys.

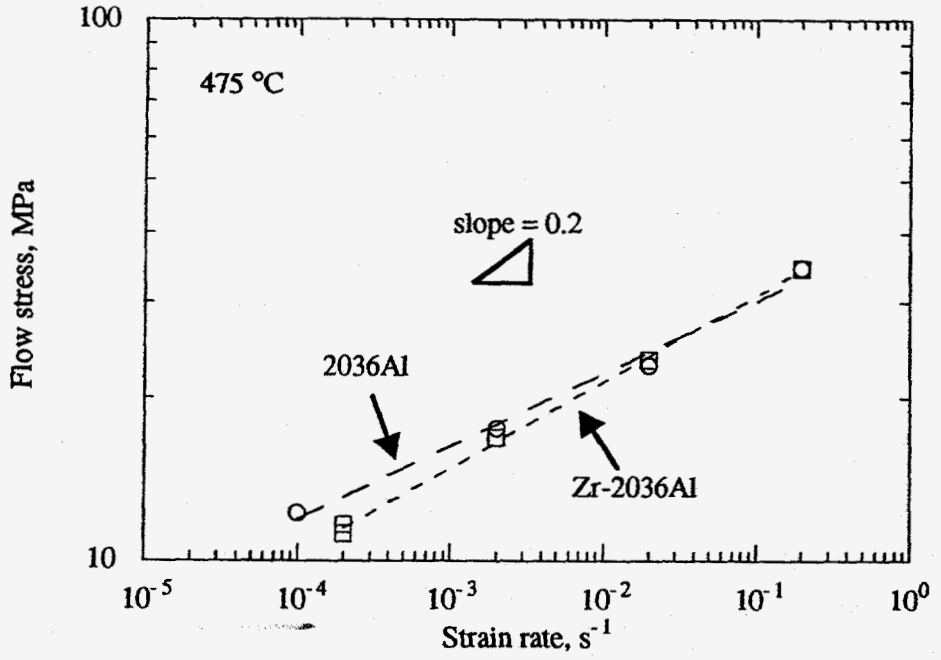

Fig. 9 Comparison of steady–state flow behavior between 2036 Al and Zr–2036 Al at 475°C.

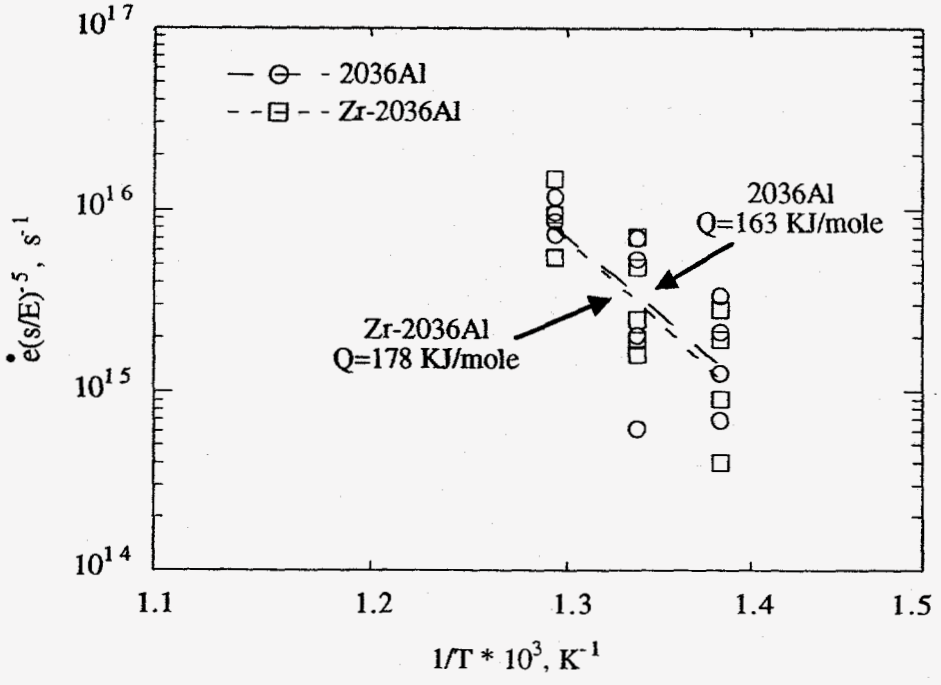

Fig. 10 Normalized strain rate as a function of the inverse temperature for both alloys.

A comparison of total elongation value at 475°C for the two alloys is shown in Fig. 11. Within the strain rate range (2×10^{-1} to 2×10^{-4} s^{-1}), elongation appears to increase only slightly with strain rate, indicating it is not a strong function of strain rate. The decreasing elongation at lower stain rates is probably caused by an increase in grain boundary cavitation. In fact, metallographic examination indicates that grain boundary cavitation becomes prevalent at strain rates $\leq 2 \times 10^{-3}$ s^{-1}. The elongation values for the two alloys are noted to be comparable, suggesting that the addition of a 0.21 wt% Zr to 2036 Al has little effect on the high–temperature deformation properties, including ductility. A higher Zr addition is apparently necessary to enhance the formability of 2036 Al.

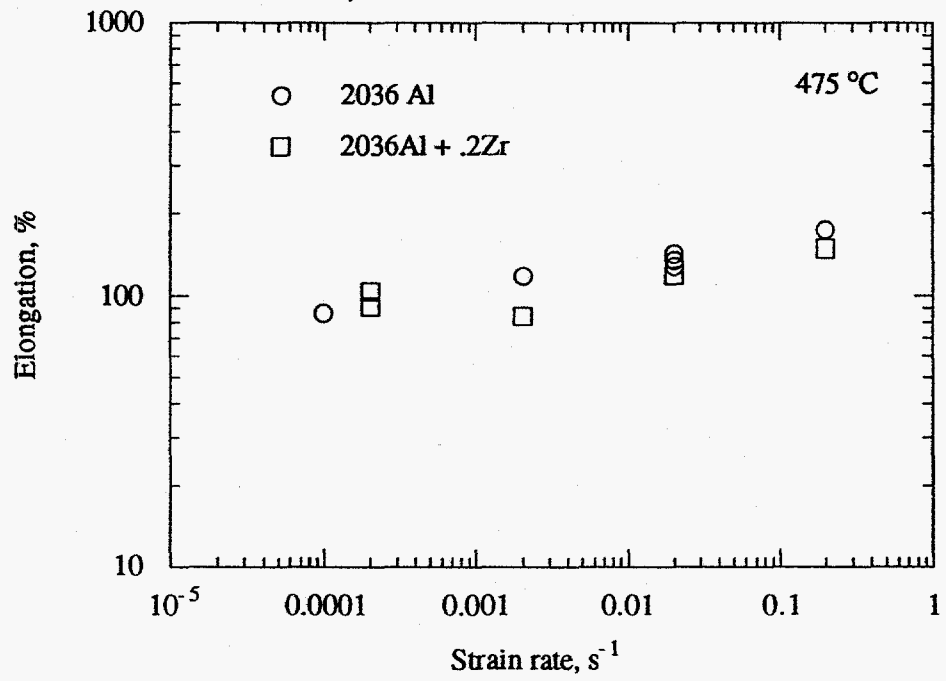

Fig. 11 Comparison of elongations versus strain rate for both alloys at 475°C.

Conclusion

The microstructure and high temperature deformation behavior of 2036 Al were characterized. A particle–simulated–nucleation (PSN) process was applied to refine the grain structure of the alloy. Within the temperature (450–500°C) and strain rate (2×10^{-1} to 2×10^{-4} s^{-1}) ranges studied, 2036 Al exhibits a strain rate sensitivity exponent of less than 0.2, and an activation energy of about 163 kJ/mol, which is close to the activation energy for self diffusion in Al, suggesting a recovery–type mechanism (e.g., dislocation climb) is responsible for high–temperature deformation. The elongation value is insensitive to strain rate and the maximum elongation of about 200% was obtained. A 0.2 wt% Zr addition to 2036 Al resulted in the precipitation of fine (20–60 nm) Al_3Zr particles. These particles were distributed primarily within grains and did not lead to grain refinement. As a result, the addition of 0.21 wt% Zr to 2036 Al does not significantly affect the high–temperature deformation as well as ductility in 2036 Al.

Acknowledgment

This work was performed under the auspices of the U.S. Department of Energy by Lawrence Livermore National Laboratory under contract No. W–7405–Eng–48. The authors would like to thank Mr. Nhan Nguyen for his technical assistance in mechanical testing.

References

1. R. Grimes, M.J. Stowell, and B.M. Watts, "Superplastic Aluminum–based Alloys," *Metals Technol.*, **3** (1976), pp. 154–160.
2. T.G. Nieh and J. Wadsworth. "Superplasticity in Aerospace Aluminum Alloys," in *Superplasticity in Aerospace–Aluminum*, pp. 194–214, ed. R. Pearce and L. Kelly, Ashford Press, Curdridge, Southampton, Hampshire, 1985.
3. T.G. Nieh and J. Wadsworth, "Effects of Zr on the High Strain Rate Superplasticity of 2124 Al," *Scr. Metall. Mater.*, **28** (1993), pp. 1119–1124.
4. W. Zheng and B. Zhang, "Superplasticity in the 2024 Al Alloy," *Mater. Sci. Lett.*, **13** (1994), pp. 1806–1808.
5. Z. Cui, W. Zhong, J. Bao, and L. Yong, "Superplastic Behavior at High Strain Rate of Warm–Rolled 2618A Commercial Aluminum Alloy," *Scr. Metall. Mater.*, **31**(10) (1994), pp. 1311–1315.
6. J. Wadsworth, G.A. Henshall, and T.G. Nieh. "Superplastic Aluminum–Lithium Alloys," in *Aluminum–Lithium Alloys III*, pp. 199–212, ed. C. Baker, P.J. Gregson, S.J. Harris, and C.J. Peel, The Institute of Metals, London, 1986.
7. M.K. Rabinovich, O.A. Kaibyshev, and V.G. Tufinov, "Superplasticity of the Aluminum Alloy V96Ts," *Metalloved Term Obrab Met.*, **3** (1978), pp. 55–59.
8. T.G. Nieh and J. Wadsworth, "Superplasticity and Superplastic Forming of Aluminum Metal Matrix Composites," *JOM*, **44**(11) (1992), pp. 46–50.
9. H. Aiko and N. Furushiro. "Influence of Zirconium on Superplastic Deformation at 573K for an Al–10wt%Mg Alloy," in *International Conference on Superplasticity in Advanced Materials (ICSAM–91)*, pp. 423–428, ed. S. Hori, M. Tokizane, and N. Furushiro, The Japan Society for Research on Superplasticity, 1991.
10. N. Furushiro and S. Hori. "Significance of High Rate Superplasticity in Metallic Materials," in *Superplasticity in Metals, Ceramics, and Intermetallics, MRS Proceeding No. 196*, pp. 385–390, ed. M.J. Mayo, J. Wadsworth, and M. Kobayashi, Materials Research Society, Pittsburgh, Pennsylvania, 1990.
11. N. Furushiro, S. Hori, and Y. Miyake. "High Strain Rate Superplasticity and its Deformation Mechanism in Aluminum Alloys," in *International Conference on Superplasticity in Advanced Materials (ICSAM–91)*, pp. 557–562, ed. S. Hori, M. Tokizane, and N. Furushiro, The Japan Society for Research on Superplasticity, 1991.
12. J.A. Wert, N.E. Paton, C.H. Hamilton, and M.W. Mahoney, "Grain Refinement in 7075 Aluminum by Thermomechanical Processing," *Metall. Trans.*, **12A** (1981), pp. 1267–1276.
13. T.S. Lundy and J.F. Murdock, "Diffusion of Al^{26} and Mn^{54} in Aluminum," *J. Appl. Phys.*, **33** (1962), pp. 1671–1677.